Supporting Material for "A kinetic model for type I and II IP_3R accounting for mode changes"

Ivo Siekmann*
Auckland Bioengineering Institute,
The University of Auckland, Auckland, New Zealand

Larry E. Wagner II, David Yule
Department of Pharmacology and Physiology,
University of Rochester Medical Center,
Rochester, New York 14642, USA

Edmund J. Crampin
Auckland Bioengineering Institute & Department of Engineering Science,
The University of Auckland, Auckland, New Zealand

James Sneyd
Department of Mathematics,
The University of Auckland, Auckland, New Zealand

July 16, 2012

*Corresponding author. Address: Auckland Bioengineering Institute, The University of Auckland, 70 Symonds St, Auckland, New Zealand, Tel.: (+64) 9 373 7599 ext. 81863, Fax: (+64)9 367 7157

1 Mathematical background

1.1 Moving average

The moving average $\hat{P}_O(i)$ for estimating the average open probability at a point i in a sequence I of current measurements from an ion channel is defined as

$$\hat{P}_O(i) = \frac{1}{w} n_O(i - w/2, i + w/2) = \frac{1}{w} \sum_{n=i-w/2}^{i+w/2} O(I^n). \tag{A1}$$

Here, $n_O(m, n)$ is the number of data points between I^m and I^n that the channel was observed to be open. $O(I)$ classifies a current I as either open, i.e. $O(I) = 1$ or closed, i.e., $O(I) = 0$ by thresholding. The window size w indicates the number of data points that were used to calculate the moving average.

In Figure S1 we show results for six traces of type II IP_3R at 10 μM IP_3, 5 mM ATP and different Ca^{2+} concentrations for a window size of $w = 500$ data points. Varying the window w over a wide range from 200 to 1,000 data points did not change the activity levels that were found.

1.2 Stationary probability distribution of Markov models

For the generator Q of a Markov model, the vector of stationary probabilities for the individual states π is obtained by solving the linear equation

$$\pi Q = 0 \tag{A2}$$

This vector π is fixed by the additional condition that its components must sum to 1. It may sometimes be easier to calculate π by taking advantage of the detailed balance constraints

$$\pi_i q_{ij} = \pi_j q_{ji}. \tag{A3}$$

1.3 Expected value, variances and standard deviations of dwell-time distributions

The densities of dwell-time distributions $f_D(t)$ for a subset $D \subset S$ of the state set S can be calculated as explained in Colquhoun and Hawkes (1). In

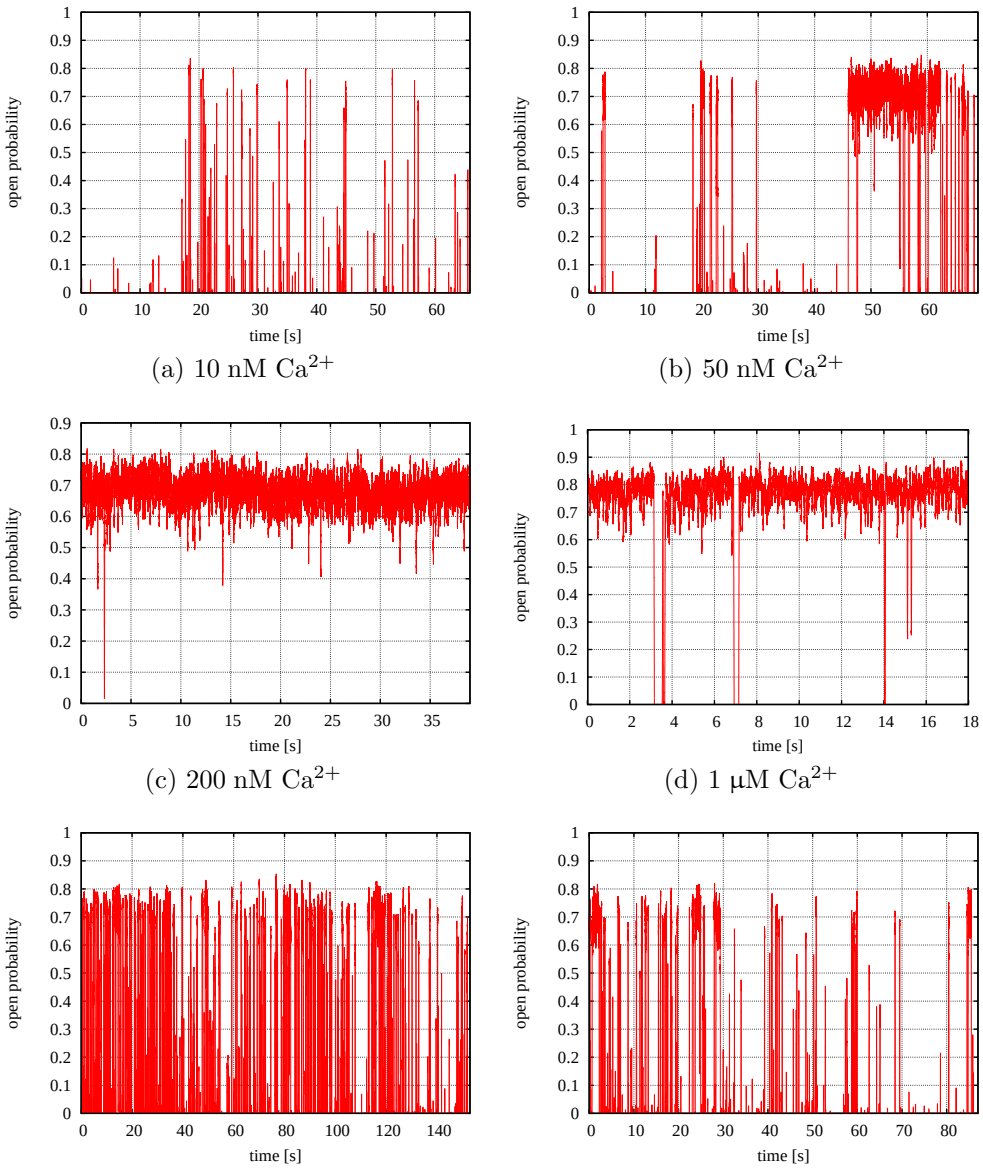

(a) 10 nM Ca^{2+} (b) 50 nM Ca^{2+}

(c) 200 nM Ca^{2+} (d) 1 µM Ca^{2+}

(e) 5 µM Ca^{2+} (f) 10 µM Ca^{2+}

Figure S1: The average open probability for data from type II IP_3R at 10 µM IP_3, 5 mM ATP, and various Ca^{2+} concentrations was estimated with moving averages over the sequence of open and closed events obtained from the data by thresholding, see equation A1. It is clearly visible that the probability $P_O^w(t)$ of the IP_3R jumps between nearly zero and approximately 70 %. The window size used here was $w = 500$ data points.

general, it is helpful to consider $f_D(t)$ as a mix of exponential distributions, i.e.,

$$f_D(t) = \sum_{i=1}^{n_D} \rho_i \frac{1}{\tau_i} \exp(-t/\tau_i). \tag{A4}$$

From the requirement $\int_0^\infty f_D(t)dt = 1$ it follows that the ρ_i are weights for n_D exponential distributions, i.e. $\sum_{i=1}^{n_D} \rho_i = 1$.

Thus, the expected value μ_D for the dwell-time τ_D in D is

$$\tau_D = \int_0^\infty t \sum_{i=1}^{n_D} \rho_i \frac{1}{\tau_i} \exp(-t/\tau_i)dt = \sum_{i=1}^{n_D} \rho_i \tau_i. \tag{A5}$$

By calculating the expected value of X^2

$$\mathbb{E}[X^2] = \int_0^\infty t^2 \sum_{i=1}^{n_D} \rho_i \frac{1}{\tau_i} \exp(-t/\tau_i)dt = \sum_{i=1}^{n_D} 2\rho_i \tau_i^2, \tag{A6}$$

the variance $\mathrm{Var}(X)$ is obtained as

$$\mathrm{Var}(\tau_D) = \mathbb{E}[X^2] - \tau_D^2 = \sum_{i=1}^{n_D} 2\rho_i \tau_i^2 - \left(\sum_{i=1}^{n_D} \rho_i \tau_i \right)^2. \tag{A7}$$

From $\mathrm{Var}(X)$ the standard deviation σ_{τ_D} is calculated by

$$\sigma_{\tau_D} = \sqrt{\mathrm{Var}(X)} = \sqrt{\sum_{i=1}^{n_D} 2\rho_i \tau_i^2 - \left(\sum_{i=1}^{n_D} \rho_i \tau_i \right)^2}. \tag{A8}$$

For dwell-times in the park and drive modes, the standard deviation σ_D is typically of a similar magnitude as τ_D, i.e., we have $\tau_D \approx \sigma_D$ which is characteristic for simple exponential distributions (rather than sums of exponentials).

1.4 Improved version of the algorithm by Siekmann et al. (2011)

The main difference to the algorithm described in Siekmann et al. (2) is that the complicated likelihood function presented there (which requires sampling a sequence of Markov states) is replaced by a simpler version, see Eq. A12. More details can be found in Siekmann et al. (3). Our aim is to infer the matrix of rate constants Q of a continuous-time Markov model for an ion channel from measured single-channel currents (I^k) of an ion channel. We

assume that points are separated by a sampling interval τ. In a first step, the sequence (I^k) is transformed to a sequence of open and closed events (E^k) by thresholding or any more advanced filtering method. Based upon the sequence (E^k) we would like to obtain the probability of a model Q. While the probability $\mathbb{P}(Q|(E^k))$ cannot be directly evaluated it can be rewritten using Bayes' theorem as

$$\mathbb{P}(Q|(E^k)) \propto \mathbb{P}((E^k)|Q)\mathbb{P}(Q), \tag{A9}$$

where $\propto$ signifies that both sides are equal up to a multiplicative constant.

The matrix $A_\tau := \exp(Q\tau)$ contains the probabilities for all transitions between a state S_i and a state S_j. This can be generalised easily for transitions between classes of states. As an example, we look at the transition from any of the open states to any of the closed states within a sampling interval τ. We can adapt our transition matrix A_τ by multiplication with the projection matrix I_O from the left-hand side and multiplying with the projection matrix I_C from the right-hand side (where I_O leaves probabilities for open states unchanged and maps probabilities for closed states to zero and I_C is analogously defined as a projection matrix to the closed states). In this way we obtain a new transition matrix

$$A_\tau^{OC} = I_O A_\tau I_C, \tag{A10}$$

G which accurately describes transitions from any of the open states to any of the closed states. If our sequence (E^k) consists of these two observations OC only, then the probability for this sequence can be calculated by

$$\mathbb{P}((OC)|Q) = \pi \cdot A_\tau^{OC} \cdot u = \pi \cdot I_O A_\tau I_C \cdot u, \tag{A11}$$

where π is the row vector of stationary probabilities of the model Q, see Eq. A2, and u is a column vector which has the value 1 in every component. Multiplication with the vector u does nothing more but summing the probabilities of exiting to any of the closed states. Note that the projection I_O ensures that the transition probability will be non-zero only if at least one of the open states has positive stationary probability.

For an arbitrary sequence (E^k), the probability $\mathbb{P}((E^k)|Q)$ can be calculated as follows:

$$\mathbb{P}((E^k)|Q) = \pi \cdot I_{E^1} \cdot A_\tau \cdot I_{E^2} \cdot \ldots \cdot I_{E^{N-1}} \cdot A_\tau \cdot I_{E^N} \cdot u, \tag{A12}$$

where each E^k is either O or C. A Metropolis-Hastings algorithm (4, 5) is then used to sample from the likelihood, see Eq. A12.

2 Kinetic models for modes

2.1 Model selection

Table S1 shows mean values and standard deviations for the results of fits to a data segment representative for the drive mode collected from type II IP_3R at 10 μM IP_3, 5 mM ATP, 0.05 μM Ca^{2+}. Models are denoted Q_{ij} where i stands for the number of closed and j for the number of open states. All models considered here are shown in Figure 2 of the main text. The likelihoods for these models indicate that model Q_{31} with three closed and one open state fits the data best—its likelihood score is higher than for models Q_{11}, Q_{21} with fewer and Q_{41} with a higher number of closed states. Models with more than one open state produced fits where all except one open states had very low stationary probabilities for one of the open states (results not shown) and therefore were excluded. Also, only one example for each of the models with one open states is shown because all topologies with one open state are equivalent (6). This lead to the conclusion that model Q_{31} is the best representation for the drive mode of the type II IP_3R. Also for different ligand concentrations and type I IP_3R data model Q_{31} achieves the highest likelihood score. For segments representative for the park mode, model Q_{11} with one open and one closed state was found to be the best representation for both receptor types (results not shown).

model Q_{ij}	q_{ij}	q_{ji}	likelihood
Q_{11}	$q_{12} = 2.684893 \pm 0.070417$	$q_{21} = 2.721870 \pm 0.072489$	-141814
Q_{21}	$q_{12} = 0.039019 \pm 0.003728$	$q_{21} = 0.086724 \pm 0.008305$	-125330
	$q_{13} = 9.787732 \pm 0.101025$	$q_{31} = 3.250568 \pm 0.035998$	
Q_{31}	$q_{12} = 1.125150 \pm 0.036311$	$q_{21} = 0.094523 \pm 0.008178$	-125072
	$q_{23} = 0.004706 \pm 0.001427$	$q_{32} = 0.011629 \pm 0.003210$	
	$q_{24} = 10.065905 \pm 0.139341$	$q_{42} = 3.272794 \pm 0.047411$	
Q_{41}	$q_{12} = 0.019692 \pm 0.007848$	$q_{21} = 0.329510 \pm 0.169228$	-125082
	$q_{23} = 0.493762 \pm 0.133622$	$q_{32} = 0.137882 \pm 0.052847$	
	$q_{34} = 1.322551 \pm 0.100999$	$q_{43} = 0.110575 \pm 0.009022$	
	$q_{45} = 10.110514 \pm 0.119087$	$q_{54} = 3.272045 \pm 0.034769$	

Table S1: Results for fits of the drive mode for a data set collected from type II IP_3R at 10 μM IP_3, 5 mM ATP, 50 nM Ca^{2+} to different models shown in Figure 2 of the main text. The mean values and standard deviations of the rate constants are given in ms^{-1}.

2.2 Probability distributions for park and drive mode

As explained in the main text (section "Submodels for modes") the results of MCMC methods are not single values such as the estimated mean values given for simplicity in Table S1 but, in fact, consist of a set of samples that can be used to approximate the probability distribution of rate constants q_{ij}. Examples for results of fits to the models that were found in the previous section to give the best representation are shown in Figures S2 (park mode) and S3 (drive mode).

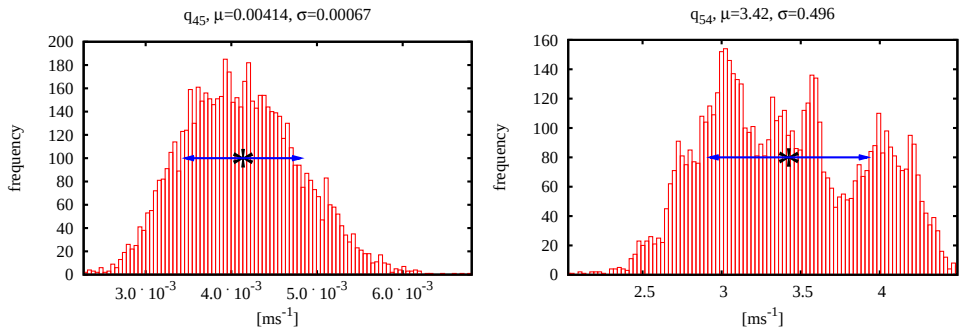

(a) q_{45} (b) q_{54}

Figure S2: Type II IP_3R: Histograms of rate constants for the inactive park mode extracted from a representative interval from a data set collected at 10 μM IP_3, 5 mM ATP, 0.05 μM Ca^{2+}. The histograms indicate how likely different values for the rate constants are based upon the data. This approximated probability distribution gives a good idea of the uncertainty of each rate constant. Mean values μ and standard deviations σ are shown above the plots and indicated in the plot by asterisks '*' and arrows. The results shown in these histograms were used for fitting the complete model (Figure 3c in the main text). The multi-modality of the histogram for q_{54} is probably a result from the very small number of openings observed in the experimental trace. Nevertheless the standard deviation is low also for this rate.

2.3 Ligand-independent kinetics

Interestingly, when park and drive mode are fitted to representative data segments at different ligand concentrations, the results are very similar, We compare results for the drive mode for data collected from type II IP_3R at 10 μM IP_3, 5 mM ATP (Figure S4). For 0.01 μM Ca^{2+} and higher calcium concentrations (5 μM and 10 μM) the results are inconclusive—the reason for this is that the data segments where the drive mode is exhibited are too short (see Figure S1) to produce reliable fits.

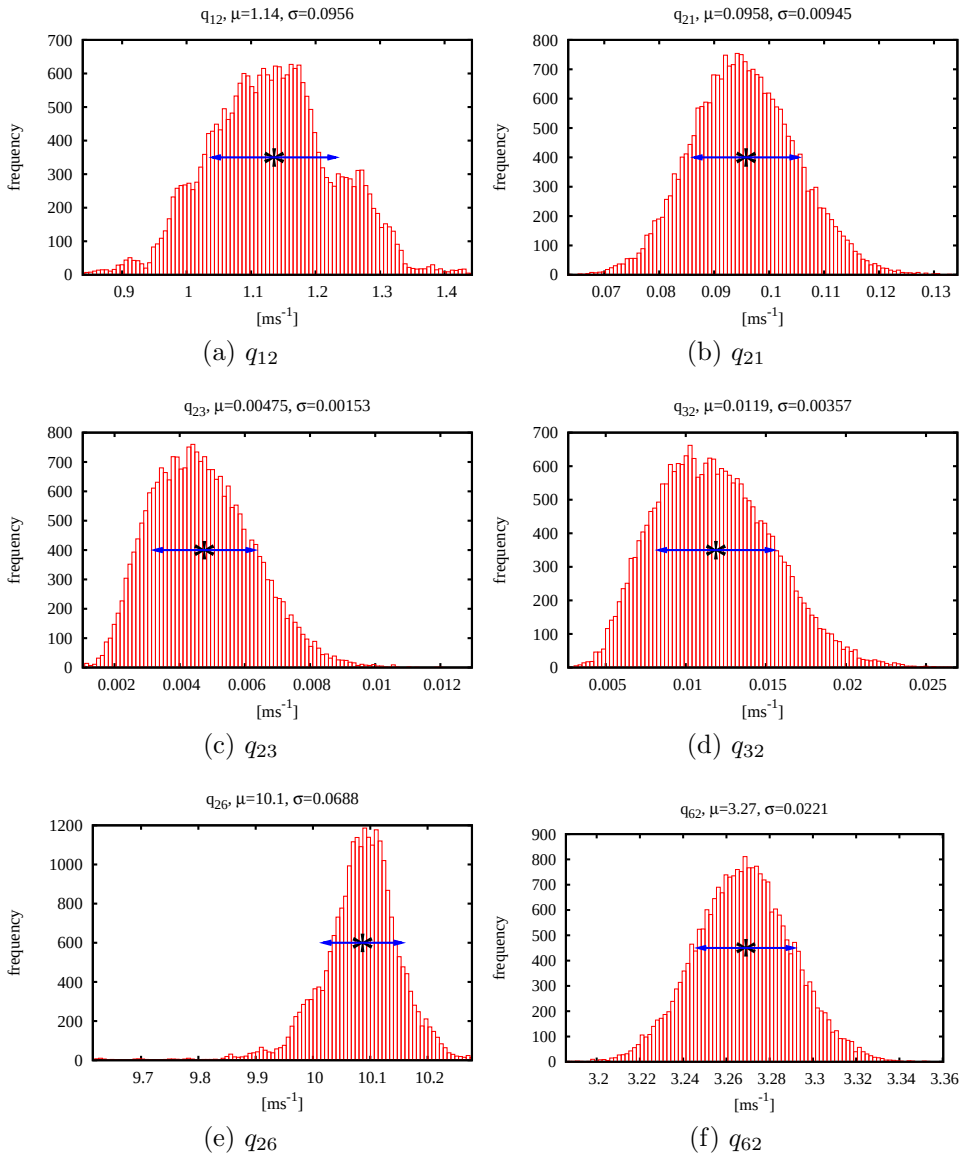

(a) q_{12} (b) q_{21}

(c) q_{23} (d) q_{32}

(e) q_{26} (f) q_{62}

Figure S3: Type II IP_3R: Histograms of rate constants for the highly active drive mode extracted from a representative interval from a data set collected at 10 μM IP_3, 5 mM ATP, 0.05 μM Ca^{2+}. The histograms indicate how likely different values for the rate constants are based upon the data. This approximated probability distribution gives a good idea of the uncertainty of each rate constant. Mean values μ and standard deviations σ are shown above the plots and indicated in the plot by asterisks '*' and arrows. The results shown in these histograms were used for fitting the complete model (Figure 3c in the main text).

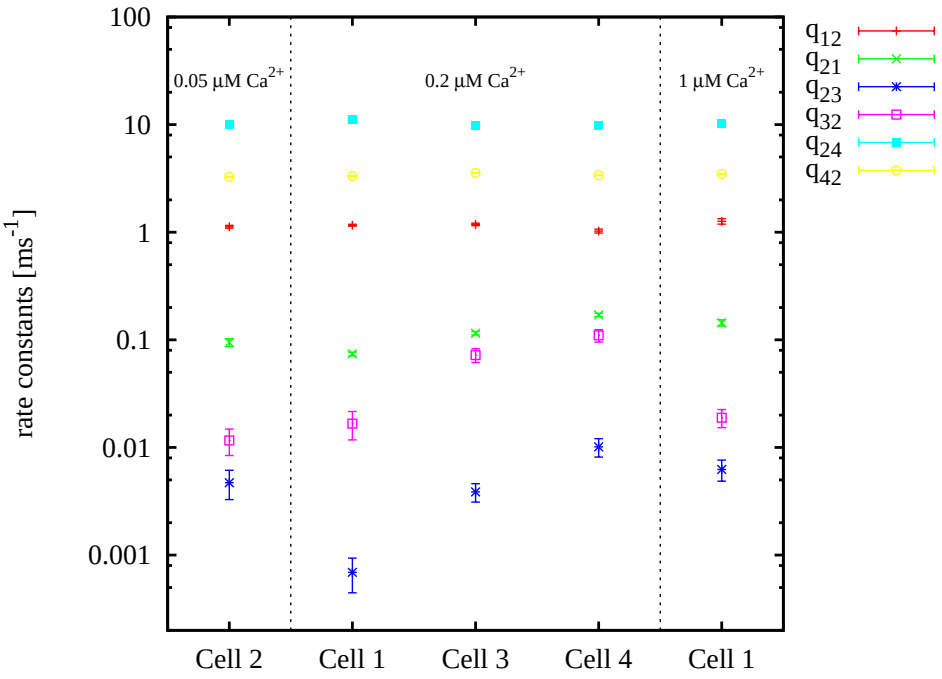

Figure S4: Means and standard deviations for the probability distributions of rate constants obtained from fits to model Q_{31} (Figure 2c in the main text) for data collected from type II IP_3R at 10 µM IP_3, 5 mM ATP and different calcium concentrations. The values are clearly similar for all three Ca^{2+} concentrations indicating that kinetics of the drive mode is ligand-independent.

3 Parameters for the complete model

The probability distributions calculated by our MCMC approach provide valuable insights into the uncertainty of each rate constant of our IP_3R model (examples are shown in Figure S2 and S3 as well as Figure 4 of the main text). In many applications, however, IP_3R models are used as components of deterministic models of calcium oscillations or stochastic models of phenomena like calcium puffs. Here, the main interest is not in the uncertainty of individual parameters but in a model that gives the correct kinetics. Therefore, it is more convenient to reduce the results to suitable point estimates such as mean values. The complete model as shown in Figure 3c in the main text consists of ligand-independent submodels for park and drive mode which are connected by transition rates q_{24} and q_{42} that depend on concentrations of IP_3, ATP and Ca^{2+}. Mean values and standard deviations for park and drive mode for both type I IP_3R and type II IP_3R are given in Table S2.

	park mode	
	q_{45}	q_{54}
Type I IP_3R	$11.1 \cdot 10^{-3} \pm 1.01 \cdot 10^{-3}$	3.33 ± 0.27
Type II IP_3R	$4.14 \cdot 10^{-3} \pm 6.7 \cdot 10^{-4}$	3.42 ± 0.496
	drive mode	
	q_{12}	q_{21}
	q_{23}	q_{32}
	q_{26}	q_{62}
Type I IP_3R	1.24 ± 0.121	0.0879 ± 0.0117
	$3.32 \cdot 10^{-3} \pm 1.64 \cdot 10^{-3}$	0.0694 ± 0.0266
	10.5 ± 0.0771	4.01 ± 0.0293
Type II IP_3R	1.14 ± 0.0956	0.0958 ± 0.00945
	$4.75 \cdot 10^{-3} \pm 1.53 \cdot 10^{-3}$	0.0119 ± 0.00357
	10.1 ± 0.0668	3.27 ± 0.0221

Table S2: Mean values and standard deviations for rate constants of the submodels representing park and drive mode (Figure 3c in the main text). All values are given in ms^{-1}

Figures 5 and 6 in the main text show the ligand-dependence of mean values and standard deviations for the transition rates q_{24} and q_{42}.

References

[1] Colquhoun, D., and A. G. Hawkes, 1981. On the stochastic properties of single ion channels. *Proceedings of the Royal Society of London B* 211:205–235.

[2] Siekmann, I., L. E. Wagner II, D. Yule, C. Fox, D. Bryant, E. J. Crampin, and J. Sneyd, 2011. MCMC estimation of Markov models for ion channels. *Biophysical Journal* 100:1919–1929.

[3] Siekmann, I., E. J. Crampin, and J. Sneyd, 2012. MCMC can detect non-identifiable models. Submitted.

[4] Metropolis, N., A. W. Rosenbluth, M. N. Rosenbluth, A. H. Teller, and E. Teller, 1953. Equation of state calculations by fast computing machines. *Journal of Chemical Physics* 21:1087–1092.

[5] Hastings, W. K., 1970. Monte-Carlo sampling methods using Markov chains and their applications. *Biometrika* 57:97–109.

[6] Bruno, W. J., J. Yang, and J. E. Pearson, 2005. Using independent open-to-closed transitions to simplify aggregated Markov models for ion channel gating kinetics. *Proceedings of the National Academy of Science of the United States of America* 102:6326–6331.